Journal of Molecular Spectroscopy **208,** 188–193 (2001)
doi:10.1006/jmsp.2001.8377, available online at http://www.idealibrary.com on IDEAL®

Reinvestigation of the Microwave Spectrum of Acetamide

R. D. Suenram,* G. Yu. Golubiatnikov,*,[1] I. I. Leonov,*,[1] J. T. Hougen,*
J. Ortigoso,† I. Kleiner,‡ and G. T. Fraser*

*Optical Technology Division, National Institute of Standards and Technology, Gaithersburg, Maryland 20899-8441; †Instituto de Estructura de la Materia, CSIC, Serrano 121, 28006 Madrid, Spain; and ‡Laboratoire de Photophysique Moléculaire, UPR CNRS 3361, Université Paris-Sud, Bâtiment 350, 91405 Orsay, Cédex, France

Received February 21, 2001; in revised form May 3, 2001; published online July 31, 2001

About 50 jet-cooled Fourier transform lines for acetamide have been recorded using a new version of our spectrometer, which has been upgraded with a heated nozzle and an expanded automatic scanning range. Nuclear quadrupole hyperfine structure arising from the nitrogen atom was removed theoretically to yield hyperfine-free center frequencies. In addition, about 30 millimeter measurements were carried out. When hyperfine structure was observed for these lines, it was also removed theoretically. A set of 115 *A*-species and *E*-species rotational transitions in the torsional ground state, obtained by combining our new measurements with the literature data, have been fit to a model involving 28 torsion, rotation, and torsion–rotation interaction parameters to near experimental uncertainty (i.e., to a weighted unitless standard deviation of 1.5), significantly improving on previous fits. Various theoretical problems associated with *K* labels for *E*-species levels in this very low barrier molecule are briefly discussed and used to justify a variant of the signed K_a labels frequently used for internal-rotor *E* states.

1. INTRODUCTION

Acetamide (CH_3–C(=O)–NH_2) has long been of spectroscopic interest as a methyl-top molecule with a very low threefold barrier and an equilibrium structure in which all of its atoms except for two of the methyl hydrogens lie in the same plane (*1–5*). Acetamide is also of interest because of the importance of the −C(=O)−NH− linkage in polypeptides. The purpose of the present work is to update the experimental data and global fit for this molecule, in preparation for planned spectroscopic investigations of small polypeptide mimetics, which often contain acetamide as a component moiety (e.g., CH_3–CH_2–O–C(=O)–CH_2–NH–C(=O)–CH_3).

The data set treated here includes: (i) microwave measurements from Toyama University (*4*), where Stark effect measurements were carried out to verify assignments, but hyperfine splittings were not treated explicitly; (ii) Fourier transform microwave measurements from Kiel (*5*), where hyperfine effects were treated theoretically to generate hypothetical hyperfine-free transition frequencies; and (iii) new Fourier transform and new millimeter-wave measurements from NIST, which were again treated to give hyperfine-free torsion–rotation transition frequencies. The data set includes only rotational transitions within the lowest ($v_t = 0$) torsional state, covering the rotational quantum number ranges $0 \le J \le 9$ and $0 \le K_a \le 7$.

A global fit of 115 transitions to 28 parameters with a root-mean-square residual of 5.3 kHz for the 57 Fourier transform measurements was carried out using a computer program described previously (*6, 7*).

The *A*- and *E*-species components of the ground torsional state of acetamide lie less than 15 cm^{-1} below the top of the low threefold barrier ($V_3 \approx 24$ cm^{-1}). The resulting near free rotor character of the ground torsional state, when combined with the noncoaxial methyl top [large value of $|D_{ab}/(A - B)| = 0.2$] and the near oblate character of acetamide ($\kappa = +0.31$), makes it difficult to assign *K* labels to *E*-species levels. In this work we use neither the very common $J_{Ka,Kc}$ labeling scheme (*8*) nor the less common J_τ labeling scheme (*8*) adopted in Refs. (*3–5*). As explained in Section 3, we use instead a new labeling scheme (*9*), which is designed to overcome some of the difficulties of the two older schemes.

2. EXPERIMENTAL

Two of our pulsed-molecular-beam Fourier transform microwave spectrometers (*10*) have been improved by equipping them with a heated nozzle and an automated wide frequency scanning capability. (The two instruments differ essentially only in having Fabry–Perot spherical mirrors with 25.4- and 30-cm radii of curvature, respectively.) Supersonic expansion in a mixture of Ne (80%) and He (20%) as carrier gas was used to cool the acetamide jet down to a temperature of 1 to 3 K.

To obtain gas-phase measurements of liquid or solid compounds, a heated pulsed nozzle was designed, as shown in Fig. 1. This nozzle is a further modification of the General Valve Series 9 type previously employed (*10, 11*). The nozzle was constructed to fit into the mirror end flange (coaxial injection geometry). A

[1] Permanent address: Applied Physics Institute of RAS, 46 Ul'yanova Street, GSP-120, Nizhny Novgorod 603600, Russia.

0022-2852/01 $35.00

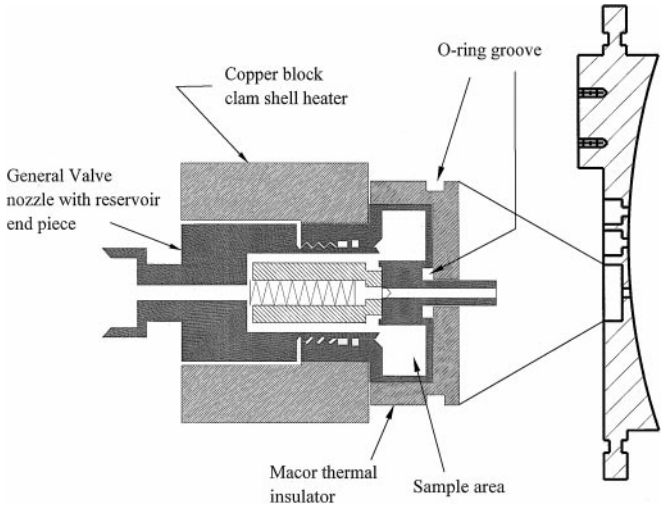

FIG. 1. Diagram of the pulsed heated General Valve nozzle with reservoir end piece, as inserted in the Fourier transform microwave spectrometer flange shown to the right.

Teflon or machinable ceramic (Macor) thermal insulator was placed between the flange and the heated reservoir (for vacuum sealing viton O-rings were used). Temperatures of 50 to 200°C were obtained by applying 15 to 40 V ac to two small cylindrical heating cartridges (Omega Engineering Inc., CSH-101100/120) built into a clamshell copper block, which fastens to the reservoir containing the heated sample. The flow of carrier gas was optimized for a given sample vaporization rate by adjusting the backing gas pressure and the tension of the valve spring.

A wide frequency scanning range of up to 3 or 4 GHz was obtained by further improvement of the automated Fabry–Perot cavity-tuning operation of the spectrometer. The new design can automatically switch from one Fabry–Perot cavity mode to another while performing a survey frequency scan, thus expanding the continuous frequency range of the scan. The mode switch occurs when the movable cavity mirror has reached the end of its maximum possible travel along the linear stage screw drive (given as a preset user-defined limit in the software). The frequency and mirror stepping is halted, the mirror is returned to its home position (at the minimum travel point), and the frequency is incremented by one step. The mirror then scans forward until the cavity is in resonance with the incremented frequency at its next (or a suitable) higher mode number, and the scan then continues as before.

For measurements in the range 78–118 GHz a precision-tunable KVARZ mm synthesizer was used directly as the source (with an output power of about 10 mW). The signal passes through a jet-cooled beam sample (using the heated nozzle mentioned above) and is focused on a high-sensitivity liquid-He-cooled InSb hot-electron bolometer (QMC). The signal-to-noise ratio and linewidths obtained should give a measurement uncertainty of 10 kHz, but some unusual lineshape problems in the spectrometer suggest that the actual uncertainty in line center determination is closer to 50 kHz.

3. ANALYSIS AND LEAST-SQUARES FIT

Predictions from refitting the 77 assigned transitions reported by Kojima *et al*. (*3, 4*) made it possible to add other transitions to the fit, and then to continue cycling in this manner. The principal disadvantage of the Toyama measurements (*3, 4*) from the present point of view is their unresolved hyperfine structure. Since hyperfine splittings can reach 1 MHz or more in this molecule, these measurements were assigned experimental uncertainties of 100 kHz in the fits. It was thus helpful to add the Heineking and Dreizler line centers determined after hyperfine interactions had been theoretically removed (*5*). Remeasurement of most of the Kiel transitions at NIST suggested that assigning a 4-kHz standard uncertainty to both the Kiel and the NIST hypothetical line centers was appropriate, except for the $3\ -1\ 3\ -3$ transition in Table 1 of Ref. (*5*), where all four frequencies listed must be decreased by exactly 1 MHz, and the $F' = 4$–$F'' = 4$ hyperfine component must be corrected for an additional misprint (our value for this 4–4 component is 23 704.857(4) MHz).

Hyperfine Splittings

To remove hyperfine shifts from the NIST measurements, our global fitting program was modified to output expectation values of $\langle J_a^2\rangle$, $\langle J_b^2\rangle$, $\langle J_c^2\rangle$, and $\langle J_a J_b + J_b J_a\rangle$ in the ρ-axis system (*12*). Putting numerical values for these quantities into the standard hyperfine energy expression,

$$E_{hf}(I, J, F) = \left[\chi_{aa}\langle J_a^2\rangle + \chi_{bb}\langle J_b^2\rangle - (\chi_{aa} + \chi_{bb})\langle J_c^2\rangle + \chi_{ab} \times \langle J_a J_b + J_b J_a\rangle\right] 2 f(I, J, F)/J(J+1), \quad [1]$$

where $f(I, J, F)$ is the Casimir function (*8*), permitted calculation of the shifts E'_{hf}—E''_{hf} of hyperfine components for each rotational transition. Values for the ρ-axis method (RAM) (*12*) hyperfine parameters in Eq. [1] determined from fitting the hyperfine patterns of 53 transitions follow the first equal signs below:

$$\begin{aligned}\chi_{aa} &= [+1.903(1)\ \text{MHz}]_{\text{RAM}} = [+1.940(1)\ \text{MHz}]_{\text{PAM}}\\ \chi_{bb} &= [+2.042(2)\ \text{MHz}]_{\text{RAM}} = [+2.005(2)\ \text{MHz}]_{\text{PAM}} \quad [2]\\ \chi_{ab} &= [-0.084(5)\ \text{MHz}]_{\text{RAM}} = [-0.104(5)\ \text{MHz}]_{\text{PAM}}.\end{aligned}$$

PAM values for the same hyperfine parameters, obtained after rotation of the RAM tensor about the c axis by an angle $\theta = (1/2)\arctan[2D_{ab}/(A-B)] = -11.035°$, are given after the second equal sign in Eq. [2] and agree well with the values of $\chi_{aa} = +1.937(2)$ MHz, $\chi_{bb} = +2.009(2)$ MHz, and $\chi_{ab} = -0.100(8)$ obtained in Ref. (*5*). (Note that the sign of χ_{ab} is not physically meaningful, since it depends on the relative choice for positive sense of the a and b axes.)

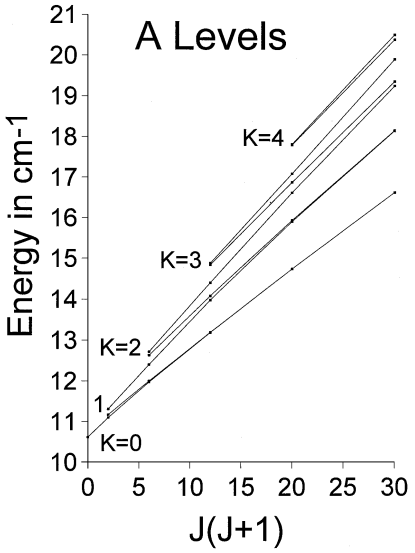

FIG. 2. *A*-species energy levels for acetamide in the torsional ground state, plotted in cm^{-1} against $J(J+1)$ for $J \leq 5$ and $K \equiv K_a \leq 4$. Note that each K_a series starts at $J = K_a$, and shows noticeable K_a-type doubling for $K_a > 0$, but that the series rapidly regroup into tight K_c clusters (K_c is not shown in the figure) with increasing J for this near oblate top ($\kappa = +0.31$). Note also that traditional J_{K_a,K_c} labeling is appropriate for these *A*-species levels, i.e., K_a increases and K_c decreases with increasing energy for given J, and that the lines connecting levels with the same K_a are nearly straight and have nearly the same slope (B value).

K Labels for Levels of E Species

Assigning K labels to levels of E species in acetamide is not entirely straightforward. The problem can be understood from a spectral analysis point of view by examining one *A*-species and two *E*-species energy level diagrams. Figure 2 shows a plot against $J(J+1)$ of *A*-species rotational levels in acetamide with $J \leq 5$ and $K_a \leq 4$. It can be seen that these levels separate nicely into series connected by relatively straight lines with almost the same slope (effective B value), and that each series can be given a K_a value by setting $K_a = J$ at the lowest J member of the series. As expected from rigid asymmetric rotor theory for a near oblate top, these K_a series increase monotonically in energy with $|K_a|$ and regroup themselves to form tight doubly degenerate K_c clusters as J increases. It is thus convenient to use rigid asymmetric rotor J_{K_a,K_c} labels for these *A*-species levels, i.e., to use J_{K_a,K_c} labels based entirely on energy ordering within a given J manifold, so that K_a increases and K_c decreases with increasing energy.

Figure 3 shows an analogous plot for *E*-species levels, again labeled with traditional J_{K_a,K_c} labels. Lines connecting J levels with the same K_a are no longer straight, so that the local effective B value (local slope) varies greatly with J. As a consequence, the frequencies of *a*-type *R*-branch transitions for the *E*-species levels in Fig. 3 can differ greatly from their *A*-type counterparts in Fig. 2. For example, the 1_{01}–0_{00} transition is at about 14 455 MHz in Fig. 2, but drops to 1100 MHz in Fig. 3, as indicated by the nearly horizontal slope of the line connecting the $J = 0$ and $J = 1$ points for the *E*-species levels with $K = 0$.

Figure 4 shows a plot of the same *E*-species levels as in Fig. 3 (apart from two $J = 5$, $|K_a| \geq 3$ points, which have $|K_a| = 5$ quantum numbers in one of the two labeling schemes), but this time the levels are connected in a different way (*9*) and labeled (as is often done (*12*) for E levels of internal rotor molecules) with signed K_a values. (Note that signed values of K_a give a complete set of $2J+1$ labels for each J, so that adding a K_c value is not necessary to make the label unique.) It can be seen that lines connecting levels of the same signed K_a are now nearly straight (well-defined B value) and have nearly the same slope (same B value), just as in Fig. 2 for the *A*-species levels. As usual, a given signed K_a series begins at $J = |K_a|$. Levels of given J no longer increase monotonically in energy with increasing $|K_a|$, however.

The physical explanation for the non-rigid-rotor energy ordering in near prolate rotors (where K_a is a relatively good quantum number) is that the Coriolis interaction between K_a rotation and internal rotation caused by the $-2F\rho P_\gamma J_z$ term in the torsion–rotation Hamiltonian splits the $|K_a|$ levels into a lower $K_a > 0$ and a higher $K_a < 0$ component (for $\langle P_\gamma \rangle > 0$), whose energy separation increases linearly with $|K_a|$. This behavior is evident for levels with $|K_a| \approx J$ in Fig. 4. In addition, the signed K_a labels correspond closely to eigenvalue composition for low J; e.g., the $J = 2$ levels in increasing energy are over 92% $K_a = +2, +1, 0, -1, -2$, respectively (which are to be compared with the rigid-rotor $|K_a|$ labels

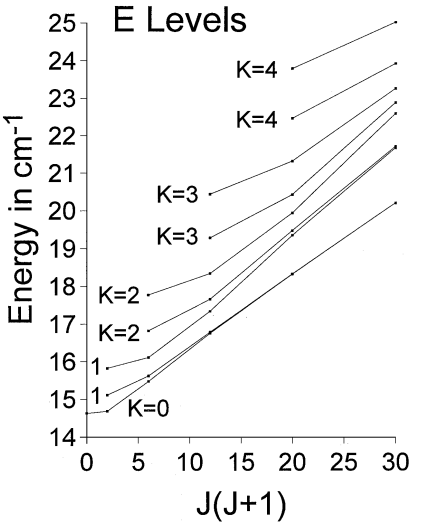

FIG. 3. *E*-species energy levels for acetamide in the torsional ground state, plotted in cm^{-1} against $J(J+1)$ for $J \leq 5$ and $K \equiv K_a \leq 4$. As in Fig. 2, the energy levels are organized into K_a series according to traditional J_{K_a,K_c} labeling, i.e., K_a increases and K_c (not shown in the figure) decreases with increasing energy for given J, and each K_a series starts at $J = K_a$. Note, however, that lines connecting levels with the same K_a are not even approximately straight, giving rise, for example, to an unusual 1_{01}–0_{00} transition frequency which is much smaller than half the 2_{02}–1_{01} frequency. Furthermore, examination of wavefunction composition shows that the level labeled 1_{01} is actually 99.6% $K_a = +1$. Thus, from both an experimental and a theoretical point of view, traditional J_{K_a,K_c} labeling is not appropriate for these acetamide torsional ground state *E*-species levels.

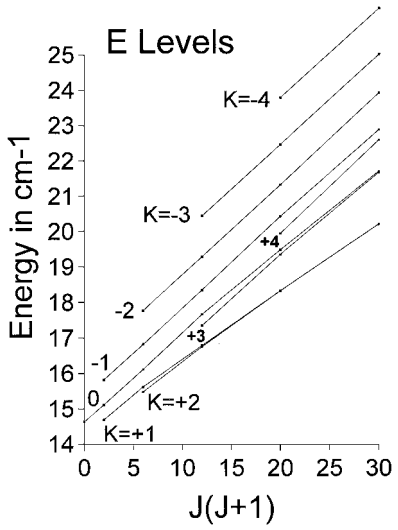

FIG. 4. The same E-species energy levels as in Fig. 3 (apart from two points with $J = 5$), but reorganized into K_a series according to Ref. (*9*). Note that lines connecting levels with the same K_a are now nearly straight and have nearly the same slope (B value), but that the energy no longer increases monotonically with $|K_a|$ for given J. Examination of wavefunction composition shows that the $J = 1$ levels labeled as $K_a = +1, 0, -1$ in this figure are over 99.6% $K_a = +1, 0, -1$, respectively, but that these percentages drop to 4, 11, and 12%, respectively, by $J = 5$. From an experimental point of view (though theoretical questions remain), the labeling in this figure is appropriate for acetamide torsional ground state E-species levels.

for the same levels of 0, 1, 1, 2, 2 in Fig. 3). The physical explanation above is not correct for high J, however, where K_c clusters are numerous, since then K_a becomes an essentially meaningless quantum number. Thus, the nominal $J = 5$, $K_a = 0$ level in Fig. 4 is only 11% $K_a = 0$; it contains in addition 16% $K_a = +5$, 10% $K_a = +4$, 30% $K_a = +3$, 9% $K_a = +1$, and 18% $K_a = -1$.

The theoretical problem is then to develop an algorithm based on eigenvector composition which leads to physically correct K_a labels when K_a is well defined, but which follows along the nearly straight lines in Fig. 4 as J increases and K_a becomes meaningless. Even though various theoretical aspects of the empirical K_a labeling scheme in Fig. 4 are still under investigation (*9*), we nevertheless adopt the scheme here. We note in passing that the authors of Refs. (*4, 5*) also abandoned J_{K_a,K_c} labels for the E-species levels shown in Fig. 3, using instead the J_τ notation (*8*), where τ is a counter increasing from $-J$ to $+J$ in order of increasing energy. We prefer the scheme used in the present paper, since the τ label (which runs over exactly the same integers as our signed K_a values) does not indicate how levels should be connected to obtain the straight lines in Fig. 4.

Final Fit

The final global fit includes 66 A-species transitions and 49 E-species transitions, giving a weighted unitless standard deviation of 1.49 using 28 adjusted parameters and no nonzero fixed parameters. This fit is a considerable improvement over earlier fits, and indicates that the model and program used are quite adequate, even for this rather low barrier of 24 cm^{-1}. Final constants from the fit of the hypothetical torsion–rotation line centers, i.e., transition frequencies with hyperfine splittings removed according to Eqs. [1] and [2], are given in Table 1. Note that the fit was carried out using the negative sign convention in $F(P_\gamma - \rho P_a)^2$, and that all transitions in the fit belong to

TABLE 1
Torsion–Rotation Parameters Obtained from the Global Fit of Hypothetical Line Centers in Acetamide

nlm[a]	Operator[b]	Parameter[b]	Value[c]	*nlm*[a]	Operator[b]	Parameter[b]	Value[c]
220	½(1-cos3γ)	V_3	24.34(1)		(1-cos3γ)(P_aP_b+P_bP_a)	d_{ab}	0.0053(1)
	P_γ^2	F	5.044(2)	413	$P_\gamma P_a P^2$	L_v	-0.122(7)×10^{-4}
211	$P_\gamma P_a$	ρ	0.08131(4)		$P_\gamma P_a^3$	k_1	0.278(3)×10^{-3}
202	P_a^2	A	0.38167(8)		$P_\gamma\{P_a,(P_b^2-P_c^2)\}$	c_4	-0.56(2)×10^{-5}
	P_b^2	B	0.31273(3)		$P_\gamma(P_a^2P_b+P_bP_a^2)$	δ_{ab}	-0.62(1)×10^{-4}
	P_c^2	C	0.16966(4)	404	$-P^4$	D_J	0.125(1)×10^{-6}
	(P_aP_b+P_bP_a)	D_{ab}	-0.0140(1)		$-P^2P_a^2$	D_{JK}	0.91(5)×10^{-6}
422	$P_\gamma^2P_a^2$	k_2	0.00266(2)		$-P_a^4$	D_K	0.657(9)×10^{-5}
	$2P_\gamma^2(P_b^2-P_c^2)$	c_1	-0.111(3)×10^{-3}		$-2P^2(P_b^2-P_c^2)$	δ_J	0.730(5)×10^{-7}
	$P_\gamma^2(P_aP_b+P_bP_a)$	Δ_{ab}	0.00136(3)		$-\{P_a^2,(P_b^2-P_c^2)\}$	δ_K	0.20(2)×10^{-6}
	sin3γ(P_aP_c+P_cP_a)	D_{ac}	0.0048(2)	624	$P_\gamma^2P^2P_a^2$	k_{2J}	0.426(7)×10^{-5}
	(1-cos3γ)P^2	F_v	0.70(2)×10^{-3}		$P_\gamma^2P_a^4$	k_{2K}	-0.95(3)×10^{-5}
	(1-cos3γ)P_a^2	k_5	−0.0391(1)	615	$P_\gamma P_a^3P^2$	λ_v	-0.55(5)×10^{-7}
	(1-cos3γ)(P_b^2-P_c^2)	c_2	-0.00232(4)		$P_\gamma P_a^5$	ℓ_k	0.706(9)×10^{-6}

[a] $n = l + m$, where n is the total order of the operator, l is the order of the torsional part and m is the order of the rotational part, respectively.

[b] {A, B} = AB + BA. The product of the parameter and operator from a given row yields the term used in the torsion–rotation Hamiltonian, except for F, ρ and A which occur in the Hamiltonian in the form $F(P_\gamma - \rho P_a)^2 + AP_a^2$.

[c] Values of the parameters from the fit shown in Table 2. All values are in cm^{-1}, except for ρ which is unitless. Type A 1σ standard uncertainties are given (i.e., $k = 1$) (*13*), in units of the least significant digit, as determined from the least-squares analysis.

TABLE 2

Assignments,[a] Observed Frequencies,[b] Uncertainties,[b] Residuals,[c] and Laboratory of Origin[d] for Hypothetical Line Centers[e] of Acetamide

J'	K_a'	K_c'	p'	J"	K_a''	K_c''	p"	Obs	(Unc)	O-C	Lab
2	2	1		1	0	1		8706.829	(4)	0.003	NIST
2	0	2		1	-1	0		9050.672	(4)	0.002	NIST
2	2	0	+	2	1	1	-	9254.418	(4)	0.002	NIST
3	2	1	+	3	2	2	-	9616.149	(4)	0.004	NIST
3	3	1		2	-1	1		12346.958	(4)	-0.002	NIST
2	1	1	-	2	1	2	+	12427.404	(4)	0.002	NIST
3	0	3		3	3	1		12587.549	(4)	0.002	HD
3	2	1	+	3	1	2	-	12678.267	(4)	-0.002	HD
2	1	1	-	2	0	2	+	13107.525	(4)	-0.002	HD
1	0	1		1	1	1		13388.703	(4)	-0.001	NIST
4	3	1	-	4	2	2	+	14210.349	(4)	0.003	NIST
3	3	0	-	3	2	1	+	14441.705	(4)	0.010	HD
1	0	1	+	0	0	0	+	14455.183	(4)	-0.003	NIST
1	0	1		0	0	0		14488.861	(4)	-0.002	NIST
4	4	1		4	0	4		14496.404	(4)	0.001	NIST
2	1	2		1	0	1		14651.888	(4)	0.005	NIST
3	3	1		3	1	3		14960.874	(4)	0.005	NIST
2	0	2		2	1	2		15115.748	(4)	-0.007	NIST
3	3	1		3	2	2		15714.277	(4)	0.002	HD
5	3	2	-	5	3	3	+	16261.362	(4)	0.011	NIST
1	1	1	+	0	0	0	+	16672.047	(4)	-0.005	HD
4	4	1		3	-2	1		16719.230	(4)	0.002	NIST
4	4	1		4	3	2		17352.782	(4)	0.002	NIST
5	4	1	+	5	3	2	-	18348.196	(4)	0.010	NIST
4	-1	3		4	4	1		18507.374	(4)	0.001	HD
3	-1	2		2	-2	0		18651.553	(4)	-0.001	NIST
2	2	1	-	2	1	2	+	19076.094	(4)	0.002	HD
6	4	2	+	6	3	3	-	19422.841	(4)	-0.008	NIST
5	3	2	-	5	2	3	+	19463.628	(4)	-0.017	NIST
2	2	1	-	2	0	2	+	19756.214	(4)	-0.002	NIST
3	-1	2		3	0	3		20686.106	(4)	0.008	HD
1	-1	0		1	0	1		20716.965	(4)	-0.003	HD
2	-1	1		2	0	2		20891.601	(4)	0.002	HD
2	0	2		2	2	1		21060.817	(4)	0.005	NIST
5	5	1		5	4	2		21218.769	(4)	-0.008	NIST
4	2	2	+	4	1	3	-	21362.138	(4)	-0.009	NIST
4	4	0	+	4	3	1	-	21762.719	(4)	-0.007	NIST
2	2	1		1	1	1		22095.527	(4)	-0.003	HD
7	5	2	-	7	4	3	+	22176.686	(4)	0.007	NIST
3	3	1	+	3	2	2	-	22769.635	(4)	0.008	HD
3	1	2	-	3	1	3	+	23566.328	(4)	0.006	NIST
3	1	2	-	3	0	3	+	23704.416	(4)	0.003	HD
5	-2	3		5	5	1		23996.933	(4)	-0.005	NIST
6	5	2		6	4	3		24013.136	(4)	0.003	NIST
2	0	2	+	1	1	1	+	24087.672	(4)	0.004	HD
5	4	2		5	0	5		24496.280	(4)	0.001	NIST
2	1	2	+	1	1	1	+	24767.791	(4)	-0.002	NIST
3	0	3		2	-1	1		24934.506	(4)	-0.001	HD
5	4	2		5	3	3		25074.295	(4)	-0.007	NIST
6	5	1	-	6	4	2	+	25149.383	(4)	-0.005	NIST
8	5	3	-	8	4	4	+	25258.902	(4)	0.001	NIST
6	6	1		6	5	2		25466.691	(4)	0.003	NIST
7	6	2		7	5	3		25665.720	(4)	0.000	NIST
3	3	1	+	3	1	2	-	25831.748	(4)	-0.004	NIST
4	-2	2		4	-1	3		26196.047	(4)	0.005	NIST
2	0	2	+	1	0	1	+	26304.533	(4)	-0.001	NIST
3	2	2	-	3	1	3	+	26628.442	(4)	-0.004	HD
3	-2	1		3	-1	2		26859.790	(100)	-0.061	KYNT
2	-2	0		2	-1	1		26969.070	(100)	0.019	KYNT
2	1	2	+	1	0	1	+	26984.790	(100)	0.131	KYNT
8	6	2	+	8	5	3	-	28030.900	(100)	-0.059	KYNT
4	3	2	+	4	2	3	-	28207.500	(100)	0.163	KYNT
7	7	1		7	6	2		28991.340	(100)	-0.094	KYNT
6	3	3	-	6	2	4	+	30094.100	(990)	0.062	KYNT
5	5	0	-	5	4	1	+	30173.900	(100)	-0.010	KYNT
5	-3	2		5	-2	3		31339.620	(100)	-0.146	KYNT
4	-3	1		4	-2	2		32141.200	(100)	-0.158	KYNT
3	2	2		2	1	2		32640.030	(100)	-0.010	KYNT
4	-1	3		4	0	4		33003.900	(100)	0.123	KYNT
3	3	1		2	0	2		33238.690	(100)	0.131	KYNT
3	1	3		2	1	2		33393.560	(100)	0.115	KYNT
5	5	1	+	5	4	2	-	33629.540	(100)	-0.136	KYNT
7	6	1	+	7	5	2	-	33742.950	(100)	-0.183	KYNT
4	-1	3		3	-2	1		35226.540	(100)	-0.061	KYNT
3	0	3	+	2	1	2	+	35674.630	(100)	0.059	KYNT
8	4	5		9	1	9		35861.930	(100)	0.059	KYNT
5	3	3	+	5	2	4	-	36099.970	(100)	-0.070	KYNT
9	7	2	-	9	6	3	+	36407.670	(100)	0.118	KYNT
3	1	3	+	2	0	2	+	36492.680	(100)	-0.106	KYNT
5	-4	1		5	-3	2		36659.670	(100)	0.169	KYNT
3	2	2		2	2	1		38585.140	(100)	0.043	KYNT
3	1	3		2	2	1		39338.450	(100)	-0.052	KYNT
2	2	1	-	1	1	0	-	39701.320	(100)	-0.067	KYNT
7	-2	5		7	-1	6		40058.000	(990)	-1.205	KYNT
3	1	2	-	2	1	1	-	40302.920	(100)	0.028	KYNT
5	3	3	+	4	2	2	+	82338.180	(50)	0.038	NIST
9	1	8	-	9	1	9	+	86920.640	(50)	0.061	NIST
9	1	8	-	9	0	9	+	86920.640	(50)	0.060	NIST
9	2	8	-	9	1	9	+	86920.640	(50)	-0.086	NIST
9	2	8	-	9	0	9	+	86920.640	(50)	-0.087	NIST
4	-2	2		3	-1	2		88282.550	(50)	0.056	NIST
4	4	0	+	3	3	1	+	89238.980	(50)	0.038	NIST
4	3	1	-	3	2	2	-	90245.830	(50)	-0.013	NIST
4	4	1		3	2	2		92566.860	(50)	-0.138	NIST
4	-3	1		3	-2	1		93563.980	(50)	-0.022	NIST
5	-1	4		4	0	4		97552.840	(50)	-0.094	NIST
7	3	5	+	6	3	4	+	97680.510	(50)	-0.010	NIST
7	3	5	+	6	2	4	+	98604.620	(50)	-0.025	NIST
5	4	2	-	4	3	1	-	99085.840	(50)	0.065	NIST
4	2	2	+	3	1	3	+	102663.960	(50)	0.017	NIST
7	3	4	-	6	4	3	-	103056.950	(50)	0.112	NIST
7	4	4	-	6	4	3	-	106033.870	(50)	-0.021	NIST
8	2	6	+	7	3	5	+	108136.930	(50)	0.083	NIST
9	1	8	-	8	2	7	-	108214.050	(50)	-0.008	NIST
9	2	8	-	8	2	7	-	108214.050	(50)	-0.155	NIST
9	1	8	-	8	1	7	-	108215.150	(50)	0.112	NIST
9	2	8	-	8	1	7	-	108215.150	(50)	-0.035	NIST
8	3	6	+	7	2	5	+	108389.300	(50)	-0.104	NIST
5	4	1	+	4	3	2	+	109194.570	(50)	0.041	NIST
4	3	2	+	3	0	3	+	110555.210	(50)	0.026	NIST
5	5	0	-	4	4	1	-	111679.650	(50)	-0.083	NIST
5	-4	1		4	-3	1		113867.640	(50)	-0.027	NIST
8	3	5	-	7	4	4	-	117020.700	(50)	0.093	NIST
8	4	4	+	7	5	3	+	117318.020	(50)	0.079	NIST
8	4	5	-	7	4	4	-	117860.770	(50)	-0.056	NIST

[a] J', K_a', and K_c' represent ordinary asymmetric rotor quantum numbers for the upper state of the transition, except that K_a' for E levels has been given a sign (*12*), and a parity p' has been added for A levels (*12*). J'', K_a'', K_c'', and p'' represent the same quantum numbers for the lower state.

[b] Observed frequencies are given in MHz; one standard uncertainty is given in kHz in parenthesis.

[c] Observed minus calculated residuals in MHz from a global fit using the parameters in Table 1.

[d] KYNT—Ref. (*4*); HD—Ref. (*5*); NIST—present work.

[e] Hypothetical line centers for NIST measurements were determined from the (usually only partially resolved) hyperfine components using the Hamiltonian and constants in Eqs. [1] and [2].

$v_t = 0$. Observed transitions (i.e., the hypothetical centers of the hyperfine patterns), assignments, and observed minus calculated residuals are given in Table 2. Note also that lines between 12 587 and 26 629 MHz in Refs. (*3*, *4*) have been remeasured using the Fourier transform technique, and that 11 lines above 29 085 MHz in Refs. (*3*, *4*) were removed from the fit because of large residuals (mostly greater than 0.5 MHz).

Presentation of hyperfine component frequencies is not warranted for our Fourier transform measurements since most components are not fully resolved in our experiments and many have measurement uncertainties only slightly smaller than the hyperfine splittings themselves. Because of this widespread blending, we have assigned standard uncertainties of 4 kHz to the hypothetical line centers in the present fit, rather than using the value of 1 kHz appropriate for well-resolved lines in our apparatus. Presentation of hyperfine component frequencies is also not warranted for our millimeter-wave measurements since, as mentioned earlier, anomalous instrumental lineshapes were often observed.

4. DISCUSSION

The high quality of the global torsion–rotation fit achieved in Table 2 for acetamide suggests that the same model and program can be applied to Fourier transform microwave data for other low-barrier molecules (in particular, polypeptide mimetics). From the point of view of internal rotation studies, however, it should be noted that no $v_t > 0$ information has been included in the fit, so that the model and fitting program have not been put to a very stringent test. Furthermore, the ratio of transitions to parameters in the fit has the rather low value of 4.1 to 1. While this is somewhat unsatisfying, it can be rationalized for small data sets in acetamide by postulating that large flectional changes occur in the planar amino group during the internal rotation motion, requiring a large number of higher-order torsion–rotation interaction terms. This ratio of 4.1 would probably improve if more J values were sampled in each K stack, since fitting the J dependence of torsion–rotation levels is traditionally much easier than fitting their K dependence.

Excited torsional levels emerge from the present fit as predicted quantities. In particular, the band centers of the A-species and E-species components of the c-type torsional fundamental vibration are predicted to lie at 1.400 and 0.584 THz, respectively. The large A–E splitting in the fundamental band arises because both symmetry components of the first excited torsional state lie above the top of the internal rotation barrier. Type B standard uncertainties (*13*) in the predicted vibrational frequencies are difficult to assess, because the uncertainties all arise from systematic model errors in a fit with a very low ratio of transitions to parameters, but it is hoped that the standard uncertainties on the two terahertz predictions are less than a few percent.

Further desirable experimental work on this molecule is of two types. First, a room-temperature microwave spectrum should be measured, so that rotational transitions at higher J and K and in several excited torsional states can be included in the analysis. Such work is currently underway (*14*). Second, the torsional $v_t = 1$–0 transition should be located. Preliminary searches using the terahertz spectrometer under construction at NIST were not successful. Whether this is due to poor frequency predictions or to insufficient spectrometer sensitivity is not yet clear.

ACKNOWLEDGMENT

The authors are indebted to Ms. Jennifer Lin for help in measuring the spectrum.

REFERENCES

1. M. Kitano and K. Kuchitsu, *Bull. Chem. Soc. Jpn.* **46,** 3048–3051 (1973).
2. R. A. Kydd and A. R. C. Dunham, *J. Mol. Struct.* **69,** 79–88 (1980).
3. T. Kojima, E. Yano, K. Nakagawa, and S. Tsunekawa, *J. Mol. Spectrosc.* **112,** 494–495 (1985).
4. T. Kojima, E. Yano, K. Nakagawa, and S. Tsunekawa, *J. Mol. Spectrosc.* **122,** 408–416 (1987).
5. N. Heineking and H. Dreizler, *Z. Naturforsch. A* **48,** 787–792 (1993).
6. I. Kleiner, J. T. Hougen, J.-U. Grabow, S. P. Belov, M. Yu. Tretyakov, and J. Cosléou, *J. Mol. Spectrosc.* **179,** 41–46 (1996). [See references therein.]
7. V. V. Ilyushin, E. A. Alekseev, S. F. Dyubko, S. V. Podnos, I. Kleiner, L. Margulès, G. Wlodarczak, J. Demaison, J. Cosléou, B. Maté, E. N. Karyakin, G. Yu. Golubiatnikov, G. T. Fraser, R. D. Suenram, and J. T. Hougen, *J. Mol. Spectrosc.* **205,** 286–303 (2001). [See references therein.]
8. C. H. Townes and A. L. Schawlow, "Microwave Spectroscopy," McGraw–Hill, New York, 1955.
9. J. Ortigoso and J. T. Hougen, work in progress.
10. R. D. Suenram, J.-U. Grabow, A. Zuban, and I. Leonov, *Rev. Sci. Instrum.* **70,** 2127–2135 (1999).
11. Certain commercial products are identified in this paper in order to specify adequately the experimental or theoretical procedures. In no case does such identification imply recommendation or endorsement by the National Institute of Standards and Technology, nor does it imply that the products are necessarily the best available for the purpose.
12. J. T. Hougen, I. Kleiner, and M. Godefroid, *J. Mol. Spectrosc.* **163,** 559–586 (1994).
13. "Guidelines for Evaluating and Expressing the Uncertainty of NIST Measurement Results," NIST Technical Note 1297, 1994, available from http://physics.nist.gov/cuu/Uncertainty/index.html.
14. V. V. Ilyushin, personal communication.